

Characterization of *Clostridium ljungdahlii* OTA1: a non-autotrophic hyper ethanol-producing strain

Jason M. Whitham¹ · Mark J. Schulte² · Benjamin G. Bobay³ ·
Jose M. Bruno-Barcena¹ · Mari S. Chinn⁴ · Michael C. Flickinger² ·
Joel J. Pawlak⁵ · Amy M. Grunden¹ 

Received: 8 July 2016 / Revised: 27 October 2016 / Accepted: 31 October 2016 / Published online: 19 November 2016
© Springer-Verlag Berlin Heidelberg 2016

Abstract A *Clostridium ljungdahlii* lab-isolated spontaneous-mutant strain, OTA1, has been shown to produce twice as much ethanol as the *C. ljungdahlii* ATCC 55383 strain when cultured in a mixotrophic medium containing fructose and syngas. Whole-genome sequencing identified four unique single nucleotide polymorphisms (SNPs) in the *C. ljungdahlii* OTA1 genome. Among these, two SNPs were found in the gene coding for AcsA and HemL, enzymes involved in acetyl-CoA formation from CO/CO₂. Homology models of the respective mutated enzymes revealed alterations in the size and hydrogen bonding of the amino acids in their active sites. Failed attempts to grow OTA1 autotrophically suggested that one or both of these mutated genes prevented acetyl-CoA synthesis from CO/CO₂, demonstrating that its activity was required for autotrophic

growth by *C. ljungdahlii*. An inoperable Wood-Ljungdahl pathway resulted in higher CO₂ and ethanol yields and lower biomass and acetate yields compared to WT for multiple growth conditions including heterotrophic and mixotrophic conditions. The two other SNPs identified in the *C. ljungdahlii* OTA1 genome were in genes coding for transcriptional regulators (CLJU_c09320 and CLJU_c18110) and were found to be responsible for deregulated expression of co-localized arginine catabolism and 2-deoxy-D-ribose catabolism genes. Growth medium supplementation experiments suggested that increased arginine metabolism and 2-deoxy-D-ribose were likely to have minor effects on biomass and fermentation product yields. In addition, in silico flux balance analysis simulating mixotrophic and heterotrophic conditions showed no change in flux to ethanol when flux through HemL was changed whereas limited flux through AcsA increased the ethanol flux for both simulations. In characterizing the effects of the SNPs identified in the *C. ljungdahlii* OTA1 genome, a non-autotrophic hyper ethanol-producing strain of *C. ljungdahlii* was identified that has utility for further physiology and strain performance studies and as a biocatalyst for industrial applications.

Electronic supplementary material The online version of this article (doi:10.1007/s00253-016-7978-6) contains supplementary material, which is available to authorized users.

✉ Amy M. Grunden
amy_grunden@ncsu.edu

- ¹ Department of Plant and Microbial Biology, North Carolina State University, 4548 Thomas Hall, Campus Box 7615, Raleigh, NC 27695-7615, USA
- ² Department of Chemical and Biomolecular Engineering, 196 Golden LEAF Biomanufacturing Training and Education Center, North Carolina State University, Raleigh, NC 27695, USA
- ³ Duke University NMR Center, Duke University Medical Center, Duke University, Durham, NC 27710, USA
- ⁴ Department of Biological and Agricultural Engineering, North Carolina State University, 277 Weaver Labs, Campus Box 7625, Raleigh, NC 27695-7625, USA
- ⁵ Department of Forest Biomaterials, North Carolina State University, 2028C Biltmore Hall, Campus Box 8001, Raleigh, NC 27695-8001, USA

Keywords Acetyl-coA · Carbon monoxide dehydrogenase · *Clostridium ljungdahlii* · Ethanol · Wood-Ljungdahl pathway

Introduction

Clostridium ljungdahlii was originally isolated in 1987 for its ability to produce ethanol from syngas components CO or CO₂ and H₂ (Barik et al. 1988; Tanner et al. 1993). To do this, *C. ljungdahlii* uses the Wood-Ljungdahl pathway to reduce CO/CO₂ to a methyl group through a series of tetrahydrofolate mediated reactions and combines this with a CO/CO₂-derived carbonyl group and CoA to form an acetyl-CoA (Drake 1994;

Ragsdale and Pierce 2008). This intermediate of the Wood-Ljungdahl pathway (also called the acetyl-CoA pathway), as well as central carbon intermediate in all organisms, can be converted to ethanol in two ways. The most energetically favorable way is conversion of acetyl-CoA to acetate by phosphotransacetylase and acetate kinase and then reduction of acetate to ethanol by aldehyde/ferredoxin oxidoreductase (AOR) and alcohol dehydrogenase (Köpke et al. 2010; Fast and Papoutsakis 2012; Mock et al. 2015). Alternatively, acetyl-CoA can be converted more directly to ethanol by a bifunctional alcohol/aldehyde dehydrogenase (Banerjee et al. 2014; Leang et al. 2013).

Today, *C. ljungdahlii* is used in industry to make cellulosic ethanol from syngas (Bengelsdorf et al. 2016; Liew et al. 2016a; Whitham et al. 2016). Other applications of *C. ljungdahlii* that are being researched and developed include microbial electrosynthesis (MES) and the carboxylate platforms (CP) (Batlle-Vilanova et al. 2015; Perez et al. 2013; Vasudevan et al. 2014). MES involves biosynthesis of chemicals from electricity, CO₂ and water (Lovley 2011; Lovley and Nevin 2011; Rosenbaum and Henrich 2014). *C. ljungdahlii* shows potential as a MES biocatalyst, as it can accept electrons from electrodes to reduce CO₂ to primarily acetate (Nevin et al. 2011; Nevin et al. 2010). CP involves fermentation of waste streams to generate short-chain fatty acids (e.g., acetate) and fatty alcohols (e.g., ethanol) which are elongated to medium-chain fatty acids (e.g., caproate) and subsequently reduced to medium-chain fatty alcohols (e.g., hexanol) (Agler et al. 2012; Agler et al. 2011). *C. ljungdahlii* can potentially fill multiple roles in CP including production of short-chain fatty acids and alcohols in the initial fermentation as well as reduction of medium-chain fatty acids after elongation (Perez et al. 2013; Vasudevan et al. 2014).

This study describes the genomic and phenotypic characterization of a strain of *C. ljungdahlii* designated as OTA1 that is able to generate more than twice as much ethanol as compared to the type strain *C. ljungdahlii* PETC (hereafter referred to as the “WT” for wild-type strain) when both were cultured in rich mixotrophic medium (Tirado-Acevedo 2010). The *C. ljungdahlii* OTA1 strain was selected after repeated subculturing of the WT strain in modified reinforced clostridial medium and storage at room temperature for several weeks. The initial objectives of this study were to identify the polymorphisms in the genome of *C. ljungdahlii* OTA1 and determine how these changes improved the ethanol yields of OTA1 compared to the WT strain. In the process of characterizing the effects of the mutations, OTA1 was identified to be a non-autotrophic mutant. This finding prompted a third objective to understand the contribution of the Wood-Ljungdahl pathway to growth and product formation in *C. ljungdahlii*. Whole-genome DNA/RNA sequencing, homology modeling of mutated enzymes, fermentation experiments, metabolite analysis, in silico flux balance analysis, and enzyme assays

were used to address these objectives. A recent study by Liew et al. showed a similar phenotype for a closely related bacterium, *Clostridium autoethanogenum*, after knocking out a homolog of one of the mutant genes we had identified in OTA1 (Liew et al. 2016b). Potential applications of the non-autotrophic OTA1 mutant or individual mutant nucleotide sequences identified within its genome are also discussed.

Materials and methods

Media and growth conditions

C. ljungdahlii ATCC 55383 (PETC strain) was obtained from the American Type Culture Collection. *C. ljungdahlii* OTA1 is a lab-isolated spontaneous-mutant strain of *C. ljungdahlii* ATCC 55383 and has been archived in the North Carolina State University Culture Collection as strain NC2009-OTA1. The strains were cultured mixotrophically in 160-ml serum bottles containing 50 ml of modified reinforced clostridial medium with 5 g/L fructose (mRCMf) and an artificial syngas headspace (110 ml; 20% CO, 20% CO₂, 10% H₂, balance N₂, or 80% CO, balance N₂) or heterotrophically with 100% N₂ headspace (Cotter et al. 2009a; Cotter et al. 2009b). The media were prepared as described in Whitham et al. (2015). Liquid samples for ethanol and acetate were taken at 12, 14, 24, 36, 48, and 72 h and were stored at –20 °C prior to analysis. Gas samples for CO, H₂, and CO₂ and liquid samples for fructose were taken at 0, 24, 36, 42, 54, and 66 h. Fructose samples were also stored at –20 °C prior to analysis, but gas was analyzed within 1 h of sampling. Two experimental replicates were performed with three biological replicates for each strain. Cells were also grown in 1YCM, which is the same as mRCMf but with no fructose, just 1 g/L of yeast extract and no other rich media components, and has an artificial syngas headspace (110 ml; 20% CO, 20% CO₂, 10% H₂, balance N₂) (Gosse et al. 2012).

Arginine and 2-deoxy-D-ribose were added to mRCM medium for supplementation experiments 12 h after inoculation of cells into experimental bottles. No acclimation with arginine or 2-deoxy-D-ribose was performed for the supplementation experiments. Stocks of 2-deoxy-D-ribose and arginine were prepared and sterilized in the same way as the growth media, and 1 ml of one of these carbon sources (0.5 g/L final concentration) was injected by syringe into the serum bottles. For arginine supplementation experiments, ammonium ion concentration in the media was measured using a Bioprofile 400 Analyzer (Nova Biomedical, Waltham, MA, USA) per the manufacturer’s instructions. To ensure that cell mass, gas and liquid products were captured at the end of the fermentation and samples were taken at 72, 96, and 120 h and analyzed as described above. Two experimental replicates were performed with three biological replicates for each strain.

Cell biocomposites were cultured as described by Schulte et al. (2016). Briefly, cells were first acclimated in 100 ml of mRCMf with an 80% CO₂/20% N₂ headspace (160-ml serum bottles), 60 h for WT and 36 h for OTA1. Cells were then transferred (2.5% v/v) to a new bottle and incubated as described above for 24 h. Cells were pelleted at 6000×g at 4 °C for 15 min, and approximately 0.0050 g of cells was extruded onto one lengthwise half (10 × 1 cm) of a 20 cm² (10 × 2 cm) pre-autoclaved strip of 3MM chromatography paper (Whatman, GE Healthcare, Little Chalfont, UK). These paper biocomposite strips were hydrated with 3 ml of 1YCM and inserted into Hungate tubes. Tubes were stoppered and removed from the anaerobic chamber. They were then crimped and flushed with an 80% CO₂/20% N₂ gas mixture and placed horizontally in the shaker at 37 °C and 100 rpm with the paper biocomposite oriented in the horizontal tubes so that the cells remained in the gas phase (not submerged in the liquid) hydrated only by the wicking action of the paper support (Fig. S1). Only a thin liquid film covered the cells, which maximizes mass transfer (Schulte et al. 2016). Gas samples were taken at 4, 12, and 24 h. This experiment was performed with three biological replicates for each strain.

Gas and liquid product analysis

Gas and liquid samples were prepared and analyzed as described previously by Whitham et al. (2015) with the following exceptions. During gas analysis, argon carrier gas was set at a flow rate of 10 ml/min, and the oven temperature was 75 °C for the first minute of the run and ramped 25 °C/min to 200 °C with no hold time. During liquid sample analysis, argon carrier gas had a flow rate of 2 ml/min, the injector temperature of the gas chromatograph was 160 °C, and the oven temperature started at 170 °C for the first 1.5 min of the run and was then ramped 75 °C/min to 240 °C and held for 3.4 min. Product analysis results were reported as an average of six biological replicates completed as triplicates of two experimental replicates.

Total carbon dioxide in the mRCMf media with syngas headspace was measured using a Bioprofile 400 Analyzer (Nova Biomedical, Waltham, MA, USA) as described by Whitham et al. 2015. A ratio of 0.2779 CO₂ liquid/CO₂ gas phase based on the values obtained for mRCMf media with a syngas headspace at 72 h was used to estimate the final CO₂ in the liquid phase of batch cultures containing mRCMf media with an initial N₂ headspace and mRCMf media supplemented with arginine or 2-deoxy-D-ribose with a syngas headspace.

Whole-genome DNA/RNA sequencing, SNP identification, and differential expression analysis

Genome sequencing and analysis were performed as previously described (Bruno-Barcena et al. 2013). Briefly,

sequencing of the *C. ljungdahlii* OTA1 genome was performed by the Genomic Science Laboratory (GSL) at NC State University and the Microbiome Core Facility at the University of North Carolina, Chapel Hill. Shotgun sequence data were generated using 454 GS FLX Titanium and Ion Torrent Personal Genome Machine (PGM) techniques. Assembly was performed using Newbler software (Roche, Basel, Switzerland) and Geneious (Biomatters, Auckland, New Zealand) with the *C. ljungdahlii* DSM 13528 sequence (accession no. CP001666) serving as the reference sequence. The assembly is deposited at NCBI Sequence Read Archive (<http://www.ncbi.nlm.nih.gov/sra>) under BioProject PRJNA298927. Geneious (Biomatters, Auckland, New Zealand) was used to identify single nucleotide polymorphisms (SNPs) within the OTA1 genome.

RNA sequencing was performed as previously described (Whitham et al. 2015). Briefly, *C. ljungdahlii* OTA1 was grown as described above in mRCMf with an artificial syngas headspace (110 ml; 20% CO, 20% CO₂, 10% H₂, balance N₂, or 80% CO, balance N₂). RNA from three biological replicates at 14 h (early log phase) and 36 h (late log phase) time points (six samples total) was processed separately into complementary DNA (cDNA). Indexed cDNA was pooled and subjected to bioanalysis prior to sequencing at the BGI and Children's Hospital of Philadelphia collaborative genome facility using the 100 bp single read protocol for one lane on the Illumina HiSeq2000. Base quality calls and demultiplexing were performed with the CASAVA 1.8.2 pipeline (Illumina, San Diego, CA, USA). RNA sequencing data for each condition was submitted to the NCBI Sequence Read Archive (<http://www.ncbi.nlm.nih.gov/sra>) under PRJNA299699. Reads were visualized with Tablet software (Milne et al. 2012).

Differential expression analysis for 14 and 36 h mixotrophically grown OTA1 and WT cultures was performed with DEGseq as described by Whitham et al. (2015). RNA sequencing data for WT cultures were produced in a previous study (Whitham et al. 2015) and is available from accession numbers PRJNA296707. Unless otherwise stated, genes mentioned in this study were significantly differentially expressed based on a false discovery rate (FDR; Benjamini and Hochberg 1995) ≤0.001 and a normalized log₂ fold change ≥4 or ≤−4.

Homology modeling of single nucleotide polymorphisms

Homology modeling was used to construct the three-dimensional models of CLJU_c37670 (WT and R528L mutant), CLJU_c09320 (WT and truncation), CLJU_c18110 (WT and truncation), and CLJU_c04490 (WT and G268V mutant) using template amino acid sequences from suitable structurally characterized X-ray crystal structures. The

following X-ray crystal structures were identified as the best templates for comparison to the four mutated OTA1 proteins: (1) the carbon monoxide dehydrogenase from *Carboxydotherrmus hydrogenoformans* for comparison with CLJU_c37670 (PDB code 3I39—E-value $2.2047E^{-146}$) (Jeoung and Dobbek 2009); (2) TrmB, a transcriptional regulator of dual function in the hyperthermophilic archaeon *Pyrococcus furiosus* for comparison with CLJU_c09320 (PDB code 3QPH—E-value $4.64464E^{-10}$) (Krug et al. 2013); (3) the full-length sorbitol operon regulator SorC from *Klebsiella pneumoniae* for comparison with CLJU_c18110 (PDB code 2W48—E-value $6.53401E^{-35}$) (de Sanctis et al. 2009); and (4) the glutamate 1-semialdehyde aminotransferase complexed with pyridoxamine-5'-phosphate from *Bacillus subtilis* for comparison with CLJU_c04490 (PDB code 3BS8—E-value $1.79373E^{-138}$) (Ge et al. 2010). Homology models were generated using MODELLER 9 version 14 (Eswar et al. 2006). During the model building process, an optimization method involving conjugate gradients and molecular dynamics to minimize violations of the spatial restraints was employed. Five hundred models were generated for each run and scored by the internal MODELLER scoring method Discrete Optimized Protein Energy (DOPE) (Shen and Sali 2006). DOPE is a statistical potential used to assess homology models in protein structure prediction. DOPE is based on an improved reference state that corresponds to non-interacting atoms in a homogeneous sphere with the radius dependent on a sample native structure; it thus accounts for the finite and spherical shape of the native structures. The structure with the lowest DOPE score was subsequently analyzed with PROCHECK and WHATCHECK to evaluate the stereochemical quality of the modeled protein structures (Hoofst et al. 1996; Laskowski et al. 1996). Molecules were visualized and aligned with PyMOL (The PyMOL Molecular Graphics System, version 1.7.4 Schrödinger, LLC.).

In silico flux balance analysis

The genome-scale model of *C. ljungdahlii* ATCC 55383 (iHN637) with constraints to simulate log-phase heterotrophic growth on fructose (Nagarajan et al. 2013) was loaded into Matlab R2015a version 8.5.0 (MathWorks, Natick, MA, USA) with the COBRA Toolbox version 2.0.6 (Schellenberger et al. 2011), libSBML version 5.11.4 (Bornstein et al. 2008), the SBMLToolbox version 4.1.0 (Keating et al. 2006), and GLPK solver version 4.55 (Department for Applied Informatics, Moscow Aviation Institute, Moscow, Russia) pre-installed. To better match the batch culture fructose consumption rate calculated with the fermentation results observed, the fructose exchange (EX_fru(e)) reaction lower limit was changed from -5 millimoles per gram of dry cell weight per hour (mmol/gDW/h) to -2.62 mmol/gDW/h. To simulate mixotrophic growth, the

lower bound of carbon monoxide exchange (EX_co(e)) and hydrogen exchange (EX_h2(e)) reactions were also set to -0.73 and -0.36 mmol, respectively. A negative value for these reactions indicates flux into the cell. The upper bounds of the carbon monoxide dehydrogenase/acetyl-CoA synthase complex (CODH_ACS) (representing AcsA) reaction and G1SAT (HemL) were constrained from 1000 to 0 mmol/gDW/h. The model objective was set to optimize for production of biomass. Solutions for 0 mmol/gDW/h flux through AcsA were loaded into an Escher (King et al. 2015) map for visualization of metabolic flux. A partial map without data loaded was used to show the predicted flux of fructose and CO₂ to ethanol and acetate for OTA1.

Acetate reductase enzyme assay

The carboxylic acid reduction (CAR) assay was performed as previously described by Whitham et al. (2015). Briefly, cell-free extracts were added to 25 °C incubated anaerobic cuvettes containing 500 mM potassium phosphate (pH 6.0), and the electron donor was methyl viologen (140 μM), which was completely reduced with dithionite (150 μM) prior to initiating the reaction. Activity was defined as micromoles of methyl viologen oxidized per minute.

Results

Single nucleotide polymorphisms identified and verified

C. ljungdahlii strain OTA1 was obtained after repeated subculturing of the WT *C. ljungdahlii* strain in a rich mixotrophic medium called mRCMf and storage at room temperature for 2 weeks. Cells from the stored culture were determined upon subsequent subculturing to support a reproducibly higher ethanol to acetate production ratio than WT. Because of this finding, OTA1 was colony purified and its fermentation profile reconfirmed. To identify the genetic basis for the higher ethanol production of OTA1 compared to WT, DNA sequencing was performed. Prior to this, OTA1 was grown in rich mixotrophic medium and verified to produce greater than a 2-fold higher yield of ethanol than WT (Fig. 1b). The acetate yield for OTA1 was also about half that observed for the WT strain, and both had about the same biomass yield (Fig. 1a, c). DNA sequencing reads from OTA1 were aligned to the *C. ljungdahlii* DSM 13528 complete genome sequence (accession no. CP001666). Eight mutations were initially identified within open reading frames (ORFs) in the OTA1 genome (Table S1). No mutations were identified in the intergenic spaces. Four of the mutations were found in both the OTA1 and WT strains (Table S1) and can be attributed to differences between DSM 13528 (the reference genome) and the genome of ATCC 55383. The other four SNPs were

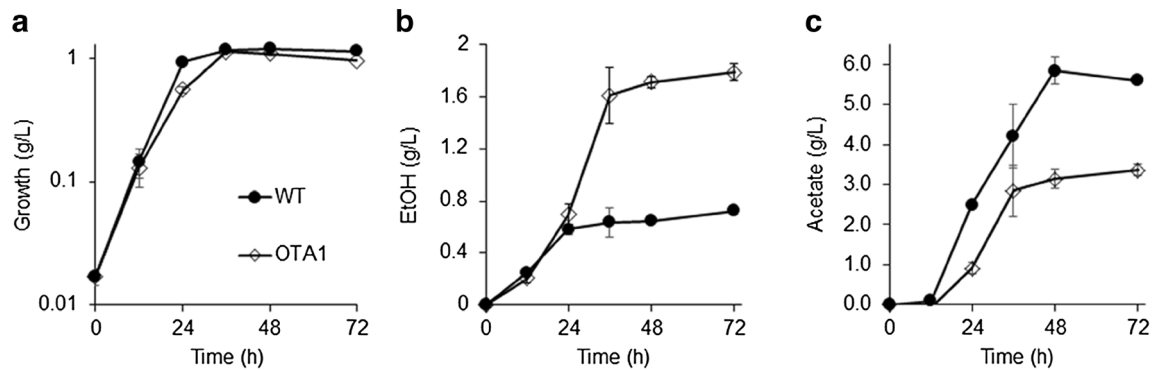


Fig. 1 Cell growth (a), ethanol (b), and acetate production (c) of *Clostridium ljungdahlii* WT (closed circle) and OTA1 strains (open diamond). One hundred sixty milliliters of batch reactors contained modified reinforced clostridial medium with 5 g/L fructose and an

artificial syngas headspace (110 ml; 20% CO, 20% CO₂, 10% H₂, balance N₂, or 80% CO, balance N₂). The data represent an average of three biological replicates per condition. Samples were taken for RNA sequencing at 14 and 36 h. Error bars indicate standard deviation

identified to be unique to the genome of OTA1 and were found to occur in genes with locus tags CLJU_c04490, CLJU_c09320, CLJU_c18110, and CLJU_c37670. These unique mutations were the only ones investigated in this study since at least one is required for the higher ethanol production by OTA1 compared to WT for mixotrophic growth conditions. All eight of the mutations were later confirmed by visualizing RNA sequencing data, generated for further strain characterization. Frequency of the mutations in mapped reads was 100%.

Table 1 summarizes the locus tag, gene name, annotation, SNP location, base change, and effects on the proteins' amino acid sequences of these unique mutations. In OTA1, CLJU_c04490 contains a mutation which changes a conserved glycine in the amino acid sequence to a valine (a polar residue to a non-polar residue). HemL (encoded by CLJU_c04490) was annotated as the only glutamate-1-semialdehyde 2,1-aminomutase in *C. ljungdahlii*'s genome, which is important for synthesis of tetrapyrrole cofactors such as cobalamin, and cobalamin is the cofactor for the corrinoid iron-sulfur protein used in acetyl-CoA synthesis (Köpke et al. 2010). CLJU_c09320 is normally translated into a protein with a DNA binding domain and a middle phospholipase D-like domain (sugar binding domain) found in TrmB

(trehalose/maltose ABC transporter) transcriptional regulators; however, in OTA1, the gene has a stop codon so that the protein only contains the DNA binding domain. While this transcriptional regulator has attributes of a TrmB transcriptional regulator, no genes co-localized with it are functionally related to trehalose/maltose transport or metabolism. Rather, it is adjacent to genes coding for enzymes that make up the arginine deiminase (ADI) pathway involved in arginine catabolism and will be referred to as the ADI transcriptional regulator in this study. Deoxyribose operon repressor (DeoR) is encoded by CLJU_c18110, and in OTA1, it is truncated so that there is no sugar binding domain. AcsA encoded by CLJU_c37670 is the key catalytic subunit of the CODH/ACS responsible for binding CO or CO₂ (which is reduced to CO) for subsequent synthesis of acetyl-CoA (Ragsdale and Pierce 2008). In OTA1, a mutation in its gene changes a conserved arginine into a leucine (a basic residue to a non-polar residue).

RNA sequencing differential expression results

To determine the impact of these mutations on gene expression, RNA sequencing and transcriptome analysis were performed by comparing samples from early (14 h) and late

Table 1 Single nucleotide polymorphisms in *Clostridium ljungdahlii* OTA1 identified by DNA sequencing and confirmed by RNA sequencing

Locus tag	Gene name	Gene annotation	Base change	Protein effect
CLJU_c04490	HemL	Glutamate-1-semialdehyde 2,1-aminomutase	G803T	G268V
CLJU_c09320	^a	Predicted transcriptional regulator	G335A	W112 ^b
CLJU_c18110	DeoR	DeoR family transcriptional regulator	T317A	L106 ^b
CLJU_c37670	AcsA	Carbon monoxide dehydrogenase	G1583T	R528L

Mutations were not found in *C. ljungdahlii* ATCC 55383

^a TrmB-like arginine deiminase (ADI) transcriptional regulator

^b Stop codon

(36 h) log phase of mixotrophically grown WT and OTA1 cultures, time points when ethanol concentration was about equal, and when there was a greater than a two times difference, respectively (Fig. 1b). Between 440 and 685 times, genome coverage was obtained for all samples. Table 2 shows all of the significantly more highly expressed genes in OTA1 as compared to WT. No genes were significantly more highly expressed in WT at 14 h, but 352 (approximately 15%) of genes were significantly more highly expressed in WT at 36 h, and most of these were annotated as spore or phage-related genes (Table S2). There were, however, expression differences in a few genes which may be involved in central carbon and ethanol metabolism including AdhE2, four hydrogenase subunits, a pyruvate formate lyase, a sugar PTS, and several transcriptional regulators. Gene-encoding proteins involved in arginine and deoxyribose catabolism adjacent to the ADI and Deo transcriptional regulators were significantly more highly expressed at both 14 and 36 h in OTA1 (Table 2). Citrate metabolism genes, citrate lyase beta chain, acyl lyase subunit (CLJU_c25330), and a citrate lyase acyl carrier protein, citrate lyase gamma chain (CLJU_c25340), were also significantly more highly expressed in OTA1 than WT at 14 h (Table 2). Neither the genes encoding for HemL or AcsA nor the other genes adjacent to these were differentially expressed. However, most of the cobalamin synthesis genes were expressed between 1- and 3-fold higher in OTA1 than WT at 36 h, and expression of the *acsA* gene was 2.19-fold higher in WT than OTA1 at 36 h (data not shown). Also, none of the known or predicted genes directly involved in ethanol, acetate, and acetaldehyde production were significantly more highly expressed in OTA1 compared to WT at 14 or 36 h (Table S3).

Homology modeling of mutated enzymes

To better understand the effects of the identified mutations, template amino acid sequences from suitable structurally characterized X-ray crystal structures were used to make homology models. The mutations in the genes coding for AcsA and HemL were found to have major effects on the enzymes' catalytic sites. The specific structural effects of the R528L mutation on AcsA can be seen in Fig. 2. The most striking effect of this mutation is the change in the number of hydrogen bonds around the mutation site. While the catalytic coordinating residue of H93 is in near identical conformation (top inset vs. bottom inset, WT vs. R528L, respectively) and is able to still interact with carbon monoxide surrogate ligand, the mutation of R528L removes the potential hydrogen bonds to D525. Investigation of all hydrogen bonds around the R528L mutation suggested that the mutation also results in the removal of potential hydrogen bonds with residues T225 and D229 (WT homology model retains these interactions).

As for HemL, the specific structural effects of the G268V mutation occur within 7–12 Å from the active binding of glutamate-1-semialdehyde. The G to V mutation results in almost twice as many intra-molecule contacts with other residues compared to WT (103 vs. 53 contacts within 4 Å—Fig. 3). However, of these residues, none are predicted to be in direct contact with the substrate as compared to substrate bound homologous protein 2ZSL. The residues potentially affected by this mutation are, however, indirectly in contact with substrate bound residues, particularly residues S113, G114, T115, and K264 (Fig. 3).

As previously mentioned, the mutations in the genes of the ADI transcriptional regulator and DeoR transcriptional regulator resulted in truncations of these enzymes such that they lack their regulatory domains (Table 1). ADI retains only its N-terminal winged helix-turn-helix motif and dimerization domain. Without its C-terminal regulatory domain, DeoR is only able to dimerize but not tetramerize, which the full-length DeoR does, resulting in an N-terminal helix-turn-helix motif dimeric protein in the case of the truncated DeoR mutant. Images of the specific structural effects are provided in Figs. 4 and 5 for the ADI transcriptional regulator and DeoR, respectively.

Functional evaluation of *C. ljungdahlii* WT and OTA1 growing under heterotrophic, mixotrophic, and supplemented mixotrophic conditions

Homology modeling showed that SNPs in the genes encoding AcsA and HemL caused alterations in their active sites (Table 1; Figs. 2 and 3). To determine if these mutations effected autotrophic growth, *C. ljungdahlii* WT and OTA1 were cultured in 1YCM, which contains less rich media components than mRCMf and no fructose. Only syngas was available as a carbon source. Though WT grew autotrophically as expected, OTA1 failed to grow on syngas alone (data not shown).

Previous studies have shown that OTA1 can deplete CO from the headspace of a batch reactor more quickly when concentrated and immobilized on a paper biocomposite than when left stirring in the liquid medium (Schulte et al. 2016; Gosse et al. 2012; Tirado-Acevedo 2010). To generate OTA1 cells for biocomposites, OTA1 had to be cultured in medium containing fructose (Schulte et al. 2016; Gosse et al. 2012). The requirement for fructose was not previously described though. In this study, it was discovered that OTA1 was a non-autotrophic strain of *C. ljungdahlii*. Since experiments were exclusively performed with OTA1, and not with WT, the difference in CO depletion has not been compared in biocomposite biocatalyst studies. CO depletion was compared between WT and OTA1 cultured in mRCMf batch cultures (Tirado-Acevedo 2010). However, CO depletion was slow in this system such that differences were indistinguishable.

Table 2 Significantly more highly expressed genes in *Clostridium ljungdahlii* OTA1 as compared to *C. ljungdahlii* ATCC 55383 grown in modified reinforced clostridial medium with 5 g/L fructose and an artificial syngas headspace (110 ml; 20% CO, 20% CO₂, 10% H₂, balance N₂, or 80% CO, balance N₂)

Early log phase (14 h)			Late log phase (36 h)		
Gene/ locus tag	Gene product	log ₂ (Fold_change) normalized	Gene/ locus tag	Gene product	log ₂ (Fold_change) normalized
CLJU_c09270 ^a	Arginine deiminase ArcA	-8.91	CLJU_c18130 ^b	Deoxyribose-phosphate aldolase	-7.54
CLJU_c18130 ^b	Deoxyribose-phosphate aldolase	-8.79	CLJU_c18120 ^b	Cytidine deaminase	-6.95
CLJU_c09280 ^a	Ornithine carbamoyltransferase	-8.58	CLJU_c18150 ^b	Phosphopentomutase	-6.26
CLJU_c09300 ^a	Carbamate kinase	-8.35	CLJU_c18140 ^b	Predicted concentrative nucleoside transporter	-6.01
CLJU_c03580	Hypothetical protein	-8.08	CLJU_c22380	Hypothetical protein	-5.51
CLJU_c09290 ^a	Predicted arginine/ornithine antiporter	-8.00	CLJU_c18170 ^b	Hypothetical protein	-5.30
CLJU_c18140 ^b	Predicted concentrative nucleoside transporter	-7.87	CLJU_c42700	18 kDa heat shock protein	-5.19
CLJU_c18120 ^b	Cytidine deaminase	-7.47	CLJU_c22290	Conserved hypothetical protein	-5.18
CLJU_c18150 ^b	Phosphopentomutase	-7.38	CLJU_c42690	18 kDa heat shock protein	-5.11
CLJU_c18170 ^b	Hypothetical protein	-7.26	CLJU_c22350	Predicted cell wall binding protein	-5.05
CLJU_c25330	Citrate lyase beta chain, acyl lyase subunit	-6.47	CLJU_c22450	Putative surface/cell-adhesion protein	-4.93
CLJU_c14610	Hypothetical protein	-6.17	CLJU_c22330	Predicted cell wall binding protein	-4.88
CLJU_c42450	Putative permease	-6.07	CLJU_c22460	Hypothetical protein	-4.80
CLJU_c18160 ^b	Pyrimidine-nucleoside phosphorylase	-5.94	CLJU_c28000	Carbamate kinase	-4.75
CLJU_c36360	Hypothetical protein	-5.90	CLJU_c09270 ^a	Arginine deiminase ArcA	-4.63
CLJU_c18540	Hypothetical protein	-5.82	CLJU_c22270	Conserved hypothetical protein	-4.56
CLJU_c05180	Conserved hypothetical protein	-5.77	CLJU_c28010	Ornithine carbamoyltransferase	-4.22
CLJU_c29510	Hypothetical protein	-5.75	CLJU_c22260	Predicted transporter protein	-4.11
CLJU_c30960	Predicted small acid-soluble spore protein	-5.73	CLJU_c22340	Putative surface/cell-adhesion protein, multiple big2 domain	-4.11
CLJU_c30990	Putative DNA methylase	-5.72	CLJU_c22220	Predicted membrane protein	-4.09
CLJU_c32380	Hypothetical protein	-5.39	CLJU_c09280 ^a	Ornithine carbamoyltransferase	-4.09
CLJU_c04140	Hypothetical protein	-5.17	CLJU_c22410	Putative membrane protein	-4.06
CLJU_c25340	Citrate lyase acyl carrier Protein, citrate lyase γ chain	-4.89			
CLJU_c30800	Hypothetical protein	-4.60			
CLJU_c00490	Hypothetical protein	-4.48			
CLJU_c28040	Transcriptional regulatory protein	-4.37			
CLJU_c28050	Predicted amino acid permease	-4.21			
CLJU_c42470	Predicted membrane protein	-4.13			
CLJU_c42460	Putative response regulatory receiver	-4.11			

A negative N.Log₂ F.C. (normalized log₂ fold change) value reflects higher expression by OTA1 than ATCC 55383

^a The gene is co-localized with CLJU_c09320

^b The gene is co-localized with CLJU_c18110

To determine if there was a difference in the rate of CO depletion, a biocomposite experiment was performed with both OTA1 and WT. Cells for each strain were first acclimated in mRCMf with an 80% CO balance N₂ headspace. From initial subculturing from freezer stocks, it took 36 h for OTA1 and 60 h for WT to reach mid-log phase, compared to 24 h for

each strain in mRCMf with headspace containing 20% CO, 20% CO₂, 10% H₂, and balance N₂. Cells were then immobilized on folded paper biocomposites, inserted into Balch tubes with minimal medium such that the biocomposites were kept moist but were not submerged in the medium, and flushed with 80% CO balance N₂

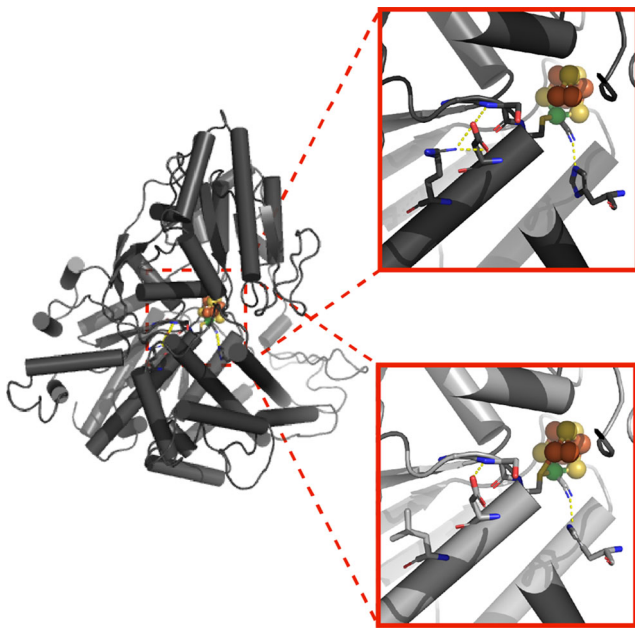


Fig. 2 Modeling of the *Clostridium ljungdahlii* OTA1 carbon monoxide dehydrogenase R528L mutation. A homology model of the non-mutant form of AcsA from *C. ljungdahlii* is shown in gray. The cylinders denote alpha helical character, while the arrows denote beta-strand character. The Fe_3NiS_4 ligand is shown as spheres; Ni is colored green. The CN ligand is shown in stick format. Atom valence is shown for clarity. The yellow lines denote the hydrogen bonds found around the active site; in particular, two are of interest, R528 and H93. R528 is of interest as it is the mutated residue, and H93 is of interest as this is the residue that hydrogen bonds with the CN ligand. The top expanded inset is showing R528 and its interactions with amino acid side chains. The bottom inset is showing the mutational effects of R528L and the lack of interactions compared to the WT sequence (color figure online)

(Fig. S1). This configuration reduced the liquid barrier for gas-liquid mass transfer and therefore faster CO depletion was observed by both strains. Figure 6 shows that OTA1

biocomposites depleted more than 93.8% of the CO from the headspace by 24 h which was faster than WT biocomposites which depleted less than 81.4% of CO from the headspace by 24 h. Figure 6 also shows that under these conditions, nearly all CO was oxidized to CO_2 for both WT and OTA1.

OTA1 was also evaluated for heterotrophic growth and compared with WT. The difference in biomass yield was about 33% less for heterotrophically-grown OTA1 compared to mixotrophically-grown OTA1 (Table 3), whereas the biomass yield was only about 10% less for heterotrophically-grown WT compared to mixotrophically grown WT. The differences between the biomass yield of OTA1 and WT fermentations was 37% less and 14% less for heterotrophic and mixotrophic conditions, respectively.

Liquid fermentation product yields were also compared. Acetate yield was 26% less for heterotrophically grown OTA1 compared to mixotrophically grown OTA1, 5% lower for heterotrophically grown WT versus mixotrophically grown WT, and 53 and 40% lower for OTA1 compared to WT under heterotrophic and mixotrophic growth conditions, respectively (Table 3). The ethanol yield was 46% higher for heterotrophically grown cultures compared to mixotrophically grown cultures of OTA1, and 200% higher for heterotrophically grown WT versus mixotrophically grown WT. Even though the percentage difference between heterotrophic and mixotrophic metabolisms for ethanol yield was greater for WT fermentations, the overall OTA1 ethanol yields were up to three times higher than those for WT fermentations (Table 3).

CO_2 yields were about the same for heterotrophically grown and mixotrophically grown OTA1 (Table 3). This was also the case for WT, but yields were lower for WT than OTA1 (Table 3). Under heterotrophic conditions, OTA1 produced 52% more CO_2 than WT (Table 3). This difference in CO_2

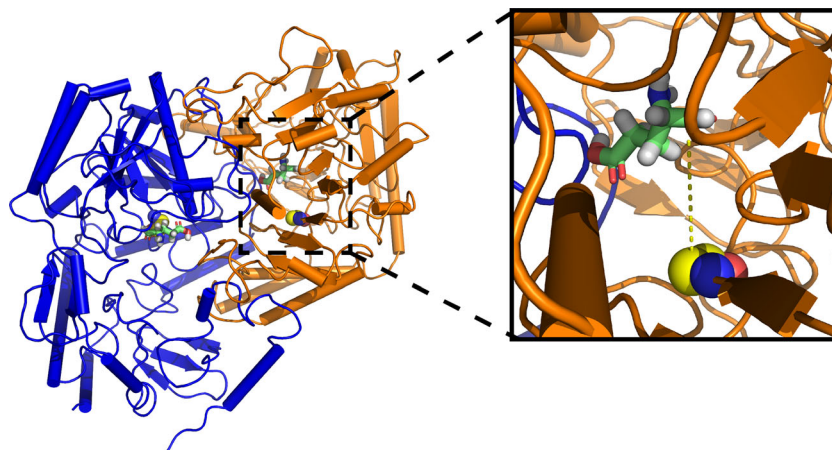


Fig. 3 Modeling of the *Clostridium ljungdahlii* OTA1 HemL G268V mutation. A homology model of the dimeric glutamate-1-semialdehyde 2,1-aminomutase (one monomer is colored blue and one is colored orange) is presented. The site of the mutation is shown as spheres with

carbons colored yellow. The substrate from a homologous characterized bound protein, glutamate-1-semialdehyde, is shown in stick format. This orientation shows how the mutation is removed from the active site (color figure online)

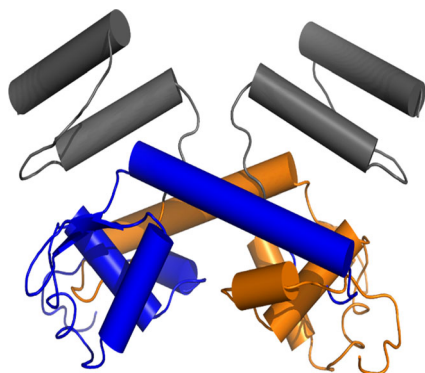


Fig. 4 Modeling of the *Clostridium ljungdahlii* OTA1 TrmB-like arginine deiminase (ADI) transcriptional regulator mutant. The ADI transcriptional regulator is a dimeric protein with an N-terminal DNA binding helix-turn-helix motif and a c-terminal regulation domain. A homology model of the ADI transcriptional regulator is shown with the c-terminal regulation domain colored gray (absent in the mutant) and the DNA binding helix-turn-helix motif colored blue (monomer one) and orange (monomer two) (color figure online)

produced by OTA1 and WT was similar for mixotrophically grown cells (65% more) (Table 3). Though more CO₂ was produced by OTA1 than WT under heterotrophic and mixotrophic growth conditions, both OTA1 and WT's CO₂ yields increased with the addition of CO and H₂ (Table 3). The difference in the total amount of CO₂ produced by OTA1 when grown mixotrophically and OTA1 grown heterotrophically was about equal to the total amount of CO consumed during mixotrophic growth when these are considered in terms of moles. In terms of grams, the CO consumed and CO₂ produced by OTA1 when grown mixotrophically was 0.479 g/L (SD = 0.003) and 2.79 g/L (SD = 0.40), respectively, and the amount of CO₂ produced by

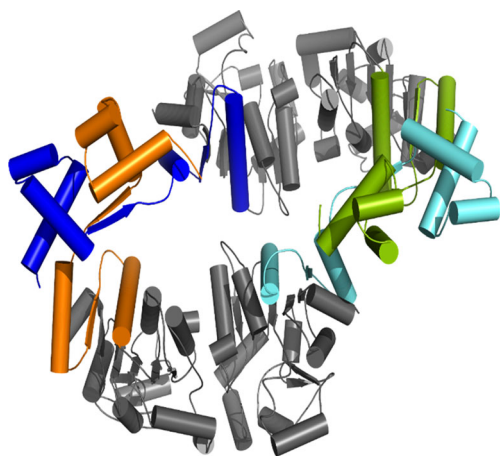


Fig. 5 Modeling of the *Clostridium ljungdahlii* OTA1 DeoR transcriptional regulator mutant. DeoR is a tetrameric transcriptional regulator protein with an N-terminal helix-turn-helix DNA binding motif and a C-terminal sugar-phosphate binding domain. A homology model of the DeoR transcriptional regulator is shown with the c-terminal regulation domain colored gray (absent in the mutant) and the DNA binding helix-turn-helix motif colored blue and orange (dimer no. 1) and green and cyan (dimer no. 2) (color figure online)

OTA1 when grown heterotrophically was 1.88 g/L (SD = 0.10). This was also true for WT. WT consumed 0.44 g/L (SD = 0.01) and produced 2.01 g/L (SD = 0.03) when grown mixotrophically, as well as produced 1.24 g/L (SD = 0.12) (data not shown). H₂ in amounts of 0.014 and 0.012 g/L were also consumed by OTA1 and WT cells when grown under mixotrophic conditions, respectively (data not shown). OTA1 and WT also produced 0.002 and 0.001 g/L H₂, respectively, under heterotrophic conditions (data not shown).

The effects of the mutated transcriptional regulators (CLJU_c09320 and CLJU_c18110) on fermentation product yields in WT and OTA1 were also investigated. Since several genes encoding arginine catabolism and 2-deoxy-D-ribose catabolism enzymes that are co-localized with the mutated transcriptional regulators were found to be significantly more highly expressed in OTA1 than WT at 14 and 36 h, both strains were cultured under mixotrophic conditions supplemented with 0.5 g of either arginine or deoxy-D-ribose to determine if metabolism of these substrates would differentially effect the fermentation product yields of WT and OTA1 (Tables 2 and 3). While arginine supplementation of the mixotrophic medium improved the ethanol yield for OTA1 by 33%, 2-deoxy-D-ribose supplementation did not affect ethanol yields for OTA1 (Table 3). Arginine supplementation also resulted in a 34% higher acetate yield than mixotrophic conditions, but 2-deoxy-D-ribose supplementation did not change acetate yields for OTA1 (Table 3). Arginine supplementation did not alter CO₂ yields for OTA1 fermentations, but 2-deoxy-D-ribose supplementation decreased the CO₂ yield by about 26% (Table 3). Both arginine and 2-deoxy-D-ribose supplementation reduced cell mass yield of OTA1 by about 39 and 28%, respectively. Both arginine and 2-deoxy-D-ribose also improved ethanol yields for WT fermentations by 0.04 and 0.03 g/g, respectively (Table 3). Though this seemed like a modest increase, it was actually a 67 and 50% yield improvement from the 0.06 g/g yield from WT under mixotrophic conditions. Neither arginine nor 2-deoxy-D-ribose supplementation greatly effect biomass, acetate, or CO₂ yields for WT fermentations (Table 3).

For all growth experiments, accurate carbon balances could not be calculated. This was because the mixotrophic medium used in these experiments contained excess rich medium components (Cotter et al. 2009a, 2009b). The sum of fermentation product and biomass yields for OTA1 ranged on average from 1.22 to 1.47 g/g defined substrates and 1.33 to 1.41 g/g for WT. Arginine-supplemented cultures had the highest total yields for both strains.

To determine if the rate of metabolism of arginine was different between WT and OTA1, NH₄⁺ in the fermentation medium was monitored since arginine catabolism produces NH₃, which is in equilibrium with NH₄⁺. Figure S2 shows

Fig. 6 CO consumed (a) and CO₂ produced (b) by biocomposites. Reactor tubes containing biocomposites (~0.0050 g cells extruded onto one lengthwise half (10 × 1 cm) of a 10 × 2 cm pre-autoclaved strip of Whatman 3MM chromatography paper). Biocomposites were hydrated in the reactor tubes with 3 ml of 1YCM and inserted into reactor tubes. CO only experiment was initiated by flushing with a 80% CO/20% N₂ gas mixture. Reactor tubes were incubated horizontally in the shaker at 37 °C and 100 rpm with the biocomposite oriented so that the cells remained in the gas phase as well as hydrated by the wicking action of the paper support. Cells for biocomposites were obtained from mid-log cultures of WT and OTA1 grown in 160-ml serum bottles containing 100 ml mRCMf with an 80% CO/20% N₂ headspace

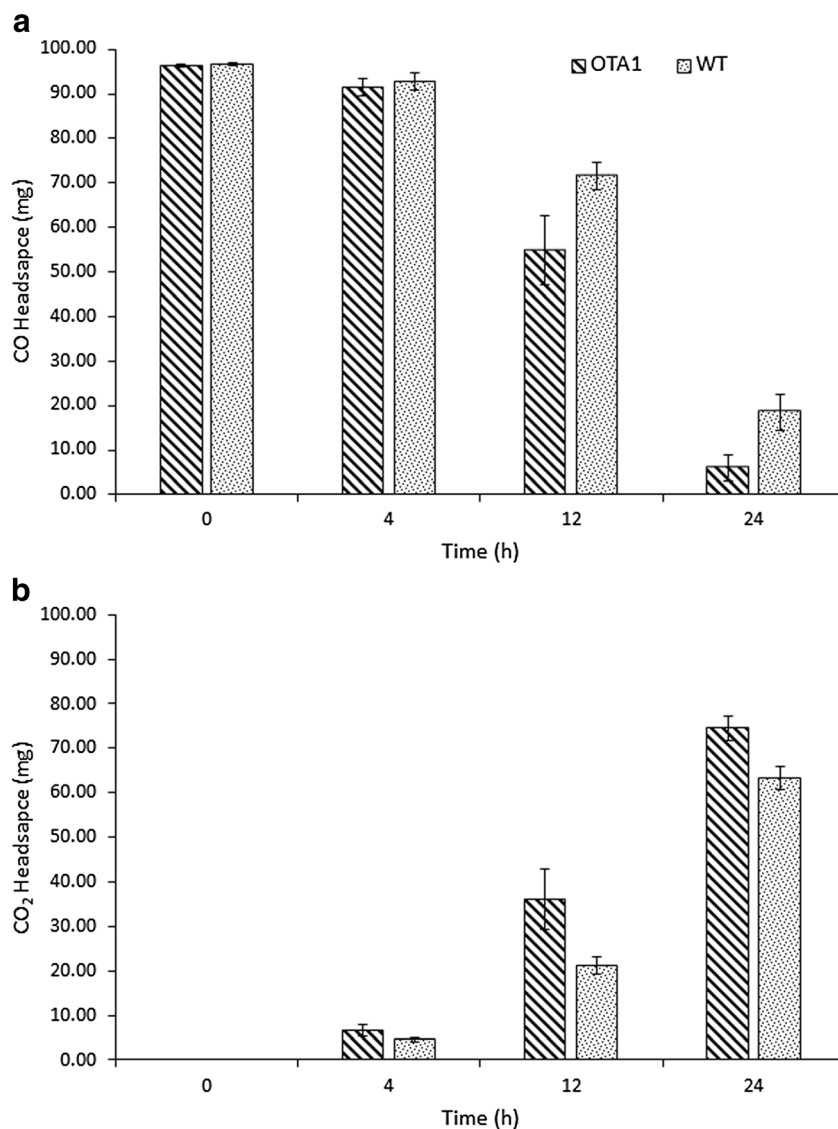


Table 3 *Clostridium ljungdahlii* WT and OTA1 product yields (grams product/grams substrate) resulting from growth under heterotrophic, mixotrophic, and supplemented mixotrophic conditions

Yields in g/g (stdev)	Heterotrophic ^b		Mixotrophic ^a		Mixo + arginine ^c		Mixo + deoxy-D-ribose ^{d,e}	
	OTA1	WT	OTA1	WT	OTA1	WT	OTA1	WT
Ethanol	0.35 (0.02)	0.18 (0.00)	0.24 (0.02)	0.06 (0.01)	0.32 (0.02)	0.10 (0.00)	0.24 (0.04)	0.09 (0.01)
Acetate	0.37 (0.02)	0.79 (0.02)	0.50 (0.03)	0.83 (0.06)	0.67 (0.04)	0.88 (0.04)	0.54 (0.05)	0.89 (0.06)
CO ₂	0.38 (0.02)	0.25 (0.02)	0.38 (0.01)	0.23 (0.01)	0.37 (0.01)	0.24 (0.01)	0.32 (0.01)	0.20 (0.01)
Biomass	0.12 (0.01)	0.19 (0.01)	0.18 (0.01)	0.21 (0.03)	0.11 (0.01)	0.19 (0.01)	0.13 (0.02)	0.20 (0.02)

^a Grams of fructose and CO consumed were considered as substrates to calculate the yield, but rich medium components were not

^b Grams of fructose consumed were considered as the substrate to calculate the yield, but rich medium components were not

^c Grams of fructose, CO, and arginine were considered as substrates to calculate the yield, but rich medium components were not

^d Grams of fructose, CO, and deoxy-D-ribose were considered as substrates to calculate the yield, but rich medium components were not

^e Ninety-six-hour time point. Seventy-two-hour time point for all other fermentation conditions

that the NH_4^+ concentration at 14 h for OTA1 was not significantly different than the NH_4^+ concentration at 72 h for WT. Furthermore, the final NH_4^+ concentration for OTA1 was about 24% higher than WT.

C. ljungdahlii OTA1 in silico flux balance analysis

To further evaluate the metabolic impact of the mutations identified in OTA1, in silico flux balance analysis was performed. The genome-scale metabolic model of *C. ljungdahlii* ATCC 55383 (iHN637) produced by Nagarajan et al. was altered by constraining the reaction rate of the acetyl-CoA synthase complex to 0 mmol/gDW/h to represent a knockout mutation of the gene encoding *AcsA*. When the HemL reaction was constrained to 0 mmol/gDW/h to represent an inactivated enzyme, the model predicted a 0 mmol/gDW/h biomass production rate for both mixotrophic and heterotrophic conditions. Therefore, only reduced activity could be simulated. Simulation of the other mutations present in OTA1 (*ADI* and *DeoR* transcriptional regulators) could not be accomplished by altering the reaction rates assumptions. The iHN637 model is constraint based, meaning that each reaction has an upper and lower bound. Many reactions have arbitrarily high default upper bounds (1000 mmol/gDW/h) and arbitrarily low default lower bounds (−1000 mmol/gDW/h). The reactions involved in arginine catabolism (arginine deiminase, ornithine carbamoyltransferase, and carbamate kinase) and reactions involved in deoxyribose catabolism (phosphopentomutase (deoxyribose) and deoxyribose-phosphate aldolase) both have arbitrarily high upper bounds. For this reason, we were unable to simulate higher reactivity due to overexpression of these genes by constraining the reaction bounds.

Maps of the metabolic flux generated from the in silico analyses data of log-phase cells cultured under heterotrophic or mixotrophic growth conditions are shown in Fig. S3. As was found in our fermentation experiments with OTA1, the model predicted no growth or metabolism for an *AcsA* gene knockout mutant under autotrophic conditions (data not shown). For both the heterotrophic and mixotrophic conditions, no ethanol production was predicted for WT and no acetate production was predicted for the *AcsA* gene knockout mutant. The *AcsA* gene knockout mutant's ethanol flux rate was slightly higher for heterotrophic conditions compared to mixotrophic conditions, 3.35 versus 3.33 mmol/gDW/h. Wild-type's acetate production rate was higher for mixotrophic conditions compared to heterotrophic conditions, 4.93 to 5.12 mmol/gDW/h. Hydrogen production was predicted for the *AcsA* gene knockout mutant (but not WT) for heterotrophic and mixotrophic conditions to be 0.33 and 1.06 mmol/gDW/h, respectively, while the CO_2 production rate for the *AcsA* gene knockout mutant

grown heterotrophically and mixotrophically was predicted to be 4.31 and 5.03 mmol/gDW/h, respectively. For WT cells grown heterotrophically or mixotrophically, the CO_2 production rate was predicted to be 0.85 or 1.05 mmol/gDW/h, respectively. Biomass production rates were forecast to be about the same for heterotrophically and mixotrophically grown cells, 0.110 mmol/gDW/h for the *AcsA* gene knockout mutant and 0.120 mmol/gDW/h for WT. Figure 7 shows the location of the *AcsA* gene knockout mutation in the context of metabolism of fructose and CO_2 to ethanol and acetate. Lower *AcsA* flux rates were also examined for mixotrophic and heterotrophic simulations in case the mutation was not a complete knockout. Flux toward higher ethanol, higher CO_2 and lower acetate were observed to change as flux through *AcsA* was reduced from 2 to 0.01 mmol/gDW/h in the mixotrophic simulation (Table S4). Unlike reduced flux for *AcsA*, reduced flux through HemL resulted in no change in flux to ethanol (remained 0 mmol/gDW/h) for both mixotrophic and heterotrophic simulations, and in heterotrophic simulations, flux to CO_2 decreased and flux to acetate increased (Table S4). Change in flux to these end products occurred gradually and at very low HemL fluxes from 0.001 to 0.000001 mmol/gDW/h (Table S4).

The model also predicted that carbon flux to ethanol for heterotrophic and mixotrophic OTA1 fermentations would come through the AOR (Fig. S3). Cell-free extracts of mixotrophically grown OTA1 and WT cells were assayed at 14 and 36 h for acetate reductase activity and were found to have about the same activity (Fig. S4).

Discussion

After multiple passages in rich mixotrophic medium and several days of storage at room temperature (~15–20 °C), a spontaneous mutant designated as OTA1 derived from the *C. ljungdahlii* ATCC 55383 type strain was produced. *C. ljungdahlii* OTA1 was isolated for further characterization because ethanol production by this strain was twice as much as WT when grown in rich mixotrophic medium (Tirado-Acevedo 2010). This phenotype was confirmed in this study (Fig. 1b).

The gene-encoding *AcsA* and HemL, critically important proteins for CO/CO_2 (C1) fixation, were found to be mutated in OTA1 (Table 1). *AcsA* is part of the acetyl-CoA synthase complex in *C. ljungdahlii*, which is the site where CO is bound or CO_2 is reduced to CO for subsequent condensation with a methyl group supplied by the corrinoid Fe-S protein (Köpke et al. 2011). Knockout of the *AcsA* encoding gene in the related bacterium, *C. autoethanogenum*, caused loss of autotrophic growth, which is one of the phenotypes observed with OTA1 (Liew et al. 2016b). In OTA1, the R528L mutation

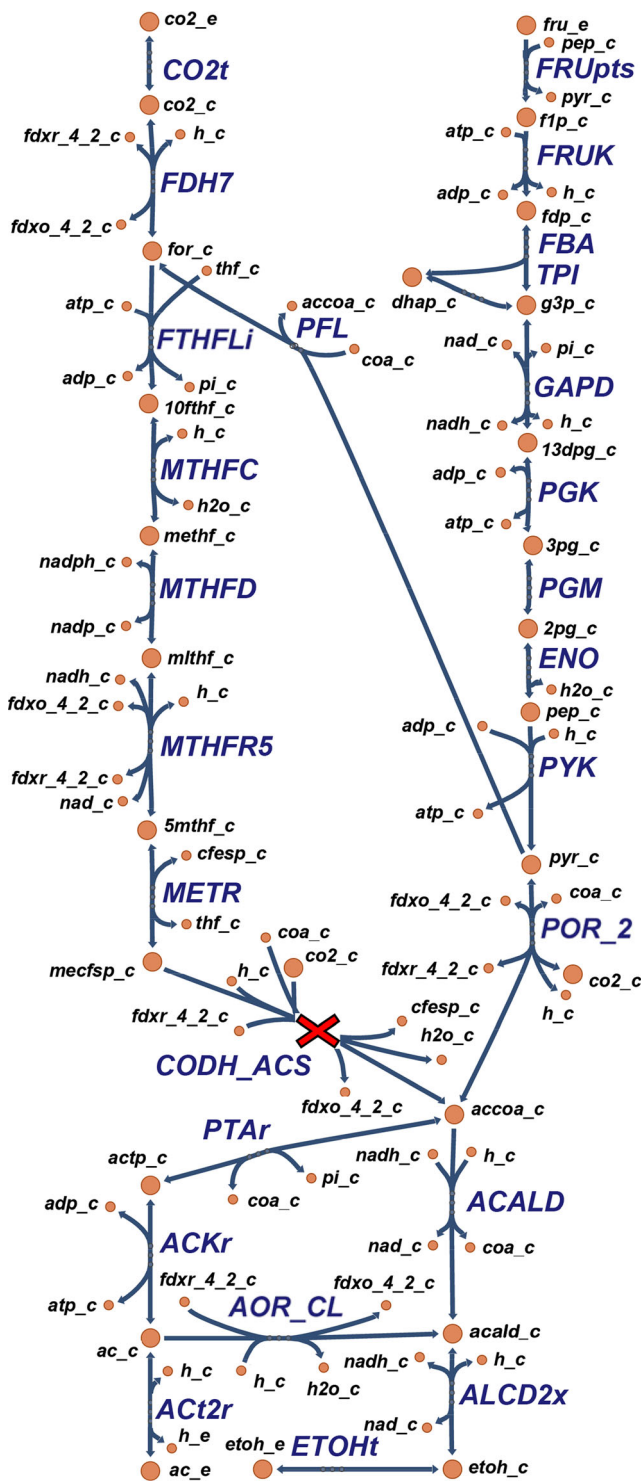


Fig. 7 Map of metabolic flux from CO₂ and fructose to ethanol and acetate in *Clostridium ljungdahlii*. The map was produced with Escher online using the IHN637 model of *C. ljungdahlii*. The red “X” indicates predicted inhibitions in metabolism due to an identified mutation in the *AcsA* gene. Metabolites and reducing equivalents: *2pg* D-glycerate 2-phosphate, *3pg* 3-phospho-D-glycerate, *5mthf* 5-methyltetrahydrofolate, *10fthf* 10-formyltetrahydrofolate, *13dpg* 3-phospho-D-glyceroyl phosphate, *ac* acetate, *accoa* acetyl-coenzymeA, *acald* acetaldehyde, *actp* acetyl phosphate, *adp* adenosine diphosphate, *atp* adenosine triphosphate, *cfesp* corrinoid iron-sulfur protein, *co2* carbon dioxide, *coa* coenzymeA, *dhap* dihydroxyacetone phosphate, *etoh* ethanol, *f1p* D-fructose 1-phosphate, *fdp* D-fructose 1,6-bisphosphate, *fdxo_4_2* ferredoxin oxidized, *fdxr_4_2* ferredoxin reduced, *for* formate, *fru* D-fructose, *g3p* glyceraldehyde 3-phosphate, *h* proton, *h2o* water molecule, *mecfsp* methylcorrinoid iron-sulfur protein, *methf* 5,10-methenyltetrahydrofolate, *mthf* 5,10-methenyltetrahydrofolate, *nad* nicotinamide adenine dinucleotide oxidized, *nadh* nicotinamide adenine dinucleotide reduced, *nadp* nicotinamide adenine dinucleotide phosphate oxidized, *nadph* nicotinamide adenine dinucleotide phosphate reduced, *pi* inorganic phosphate, *pep* phosphoenolpyruvate, *pyr* pyruvate, and *thf* tetrahydrofolate. A “c” at the end of metabolite codes refers to intercellular, while an “e” refers to extracellular. Enzymes: *ACKr* acetate kinase, *ACALD* acetaldehyde dehydrogenase, *ACT2r* acetate transport, *ALCD2x* alcohol dehydrogenase, *AOR_CL* aldehyde oxidoreductase, *CO2t* CO₂ diffusion, *CODH_ACS* carbon monoxide dehydrogenase/acetyl-CoA synthase, *ENO* enolase, *ETOHt* ethanol transport, *FBA* fructose-bisphosphate aldolase, *FDH7* formate dehydrogenase, *FRUK* fructose-1-phosphate kinase, *FRUpts* D-fructose PTS transport, *FTHFLI* formate-tetrahydrofolate ligase, *GAPD* glyceraldehyde-3-phosphate dehydrogenase, *METR* methyltetrahydrofolate/corrinoid iron-sulfur protein methyltransferase, *MTHFC* methenyltetrahydrofolate cyclohydrolase, *MTHFD* methylenetetrahydrofolate dehydrogenase, *MTHFR5* 5,10-methylenetetrahydrofolate reductase, *PFL* pyruvate formate lyase, *PGK* phosphoglycerate kinase, *PGM* phosphoglycerate mutase, *POR_2* pyruvate/ferredoxin oxidoreductase, *PTAr* phosphotransacetylase, *PYK* pyruvate kinase, and *TPI* triose-phosphate isomerase (color figure online)

in *AcsA* alters the hydrogen bonding pattern within the catalytic cleft of the enzyme likely leading to lower or no CO/CO₂ binding (Table 1; Fig. 2). HemL (the only annotated glutamine-1-semialdehyde 2,1-aminomutase) is integral to synthesis of the cobalamin cofactor for the corrinoid Fe-S

protein (Köpke et al. 2010). A mutation in the *hemL* gene (G268 V) in OTA1 is predicted to reduce accessibility of the substrate, L-glutamate-1-semialdehyde, by structural repositioning of multiple residues within the catalytic cleft (Table 1; Fig. 3). One of the affected residues (K264) resides in a homologous position of a known mutation in *Escherichia coli* glutamate 1-semialdehyde aminotransferase (K265R) that reduces the activity of a homologous protein by 98% (Ilag and Jahn 1992). In silico modeling supports either no effect of the mutation or limited accessibility of the substrate since complete inaccessibility results in no biomass formation. Only a very low HemL activity is required for unaltered metabolic flux rates though (Table S4). Metabolite flux rates were altered at much higher flux rates of *AcsA* (100-fold higher) than HemL (Table S4). Therefore, the mutated *AcsA* likely has a greater effect than the mutated HemL has on CO/CO₂ fixation.

The inability of OTA1 to recapture CO₂ through the Wood-Ljungdahl pathway seemed to be the most influential phenotypic effect of the mutations. Common trends of higher yields of CO₂ and ethanol and lower yields of biomass and acetate for OTA1 compared to WT fermentations were observed for

all growth conditions studied, and these trends were supported by *in silico* mixotrophic and heterotrophic simulations (Table 3; Fig. S3). *AcsA* knockout simulations specifically supported the fermentation product analyses. Reduction of flux through the *HemL* actually did not have an effect on flux to ethanol for all simulations, and flux to CO_2 was reduced while flux to acetate was increased for heterotrophic conditions, further emphasizing the limited effect of the *HemL* mutation on the phenotype of OTA1. Beside *in silico* demonstrations, the fermentation trends also can be predicted. If less CO_2 is recaptured, then fewer reducing equivalents are utilized for that purpose, and the production of ethanol is a sink for oxidation of the reducing equivalents. H_2 was also produced by OTA1 and WT during heterotrophic growth indicating that it too was used as a sink for reducing equivalents under those conditions but not under mixotrophic conditions (data not shown). Also, with less carbon from CO_2 recapture and less ATP from acetate production, there is less biomass production. OTA1 may compensate for less ATP from acetate production with ATP from increased metabolism of arginine from the rich mRCMf medium as suggested by increased production of ammonium (Fig. S2). Higher ethanol yields due to arginine supplementation in mixotrophic medium also showed that increased arginine metabolism might have some influence on OTA1's phenotype of higher ethanol yields, but the supplementation of arginine also resulted in an even greater increase in acetate yield compared to mixotrophic OTA1 fermentations (Table 3). Therefore, rapid metabolism of arginine as a result of the mutation in the transcriptional regulator for the *ADI* operon did not cause the general fermentation product trends previously mentioned. Also, supplementation of mixotrophic medium with 2-deoxy-D-ribose had little effect on any of the fermentation product yields. The only obvious effect that it had was causing OTA1's biomass yield to be reduced by about 28% (Table 3). While more rapid metabolism of a component of DNA (2-deoxy-D-ribose) as a result of the deregulated overexpression of the *deo* operon could cause reduced growth, it is unclear why adding 2-deoxy-D-ribose to a fermentation would lower growth even more (Table 3). The general trends in fermentation products observed are therefore most readily explained by the mutation in the gene encoding *AcsA* and a resulting inoperable Wood-Ljungdahl pathway. This conclusion is supported by Liew et al. study which showed that knockout of the *AcsA* gene in *C. autoethanogenum* not only eliminated CO/CO_2 fixation but also nearly eliminated acetate, increased ethanol, and increased CO_2 production when grown heterotrophically and mixotrophically (Liew et al. 2016b).

Complementing and expanding on Liew et al.'s work, this study provides additional insights on carbon and electron flux by using differential expression analysis, *in silico* flux analysis, and enzyme activity assays. The driving force for higher ethanol production and lower acetate production by OTA1 compared to WT is not increased gene expression of enzymes

related to ethanol and acetate production, but instead, the requirement for reoxidation of reduced electron carriers (NAD(P)H, ferredoxin, etc.) for continued metabolism. The *in silico* flux balance analysis of the *AcsA* knockout mutant predicted that carbon flow to ethanol only went through the aldehyde ferredoxin oxidoreductase (AOR) to generate the precursor of ethanol, acetaldehyde (Fig. S3). The acetaldehyde is then converted to ethanol by *AdhE1* (Fig. S3). Differential expression analysis showed that expression of *AOR* and *AdhE1* genes was either about the same or greater in WT than OTA1 at 14 and 36 h (Table S3). Also, AOR enzyme activity assays of cell-free extracts at these time points showed that acetate reductase activity was about the same for WT and OTA1 (Fig. S4). Therefore, though flux to ethanol comes through AOR, higher flux is not because of more AOR enzyme. Rather, the surplus of reduced ferredoxin generated by fructose metabolism, but not utilized for CO_2 fixation, drives flux to ethanol (Köpke et al. 2010; Mock et al. 2015). This is supported by the findings of Richter et al. that AOR and *AdhE1* protein levels in WT *C. ljungdahlii* are constantly abundant, even during acidogenesis, and surplus-reducing equivalents are shunted toward ethanol production when undissociated acetate concentrations reach a thermodynamic threshold (Richter et al. 2016). Ethanol is also formed from acetyl-CoA by the bifunctional aldehyde/alcohol dehydrogenase (*AdhE1*) (Banerjee et al. 2014; Köpke et al. 2010; Leang et al. 2013). While flux through AOR is more energetically favorable, some flux goes through *AdhE1* because of a surplus of NADH not utilized in energy conservation reactions to reduce NADP⁺, ferredoxin, or other electron carriers for CO_2 fixation drives NADH-dependent acetaldehyde and alcohol dehydrogenase activities of *AdhE1* (Mock et al. 2015; Fast and Papoutsakis 2012; Schuchmann and Müller 2014).

OTA1 cell extracts were previously shown to have on average four times higher NADH concentrations than WT cell extracts at the 14 h into mixotrophic fermentations (Tirado-Acevedo 2010). The NADH-dependent acetaldehyde activity also requires acetyl-CoA, which may be more available in OTA1 because of downregulation of a pyruvate formate lyase gene at 36 h compared to WT. If the pyruvate formate lyase works in the reverse direction as previously suggested, and as suggested by our expression data is less abundant, the pyruvate formate lyase would convert less acetyl-CoA and formate to pyruvate (Zelcbuch et al. 2016). Also, the genes encoding acetate production enzymes had about the same expression levels for OTA1 and WT at 14 and 36 h (Table S3).

Though the expression of genes coding for enzymes producing ethanol and acetate are not regulated, some energy metabolism genes were. Genes *CLJU_c28660-70*, *CLJU_c14700*, and *CLJU_c14720* encoding two putative [NiFe]-hydrogenase subunits *HyaBA* and two subunits of a putative [FeFe]-hydrogenase with homology to the *Acetobacterium woodii* *HydA* and *HydC*, respectively, were

downregulated in OTA1 compared to WT at 36 h (Table S2). Little is known about the biological function of several putative [NiFe] and [FeFe]-hydrogenases in *C. ljungdahlii* and related acetogens; however, based on homology, this [FeFe]-hydrogenase is thought to bifurcate electrons from H₂ to reduce ferredoxin and NAD⁺ (Tremblay et al. 2012; Wang et al. 2013; Buckel and Thauer 2013; Schuchmann and Müller 2014). If this is the case, transcriptional downregulation in OTA1 could be a mechanism to prevent further reduction of limited pools of reducing equivalents though it should be noted that hydrogen was nearly completely utilized in WT and OTA1 fermentations by 36 h (data not shown). Thus far, only an electron-bifurcating ferredoxin- and NADP-dependent hydrogenase has been characterized in the closely related *C. autoethanogenum* when it was cultured with high concentrations of carbon monoxide (Wang et al. 2013). In addition to supporting the point that flux toward ethanol is driven by reducing equivalents generated upstream, the regulation of these genes provides a new line of evidence for the biological function of this [FeFe] hydrogenase for generating reducing equivalents from H₂ for CO₂ reduction during autotrophic growth (Wang et al. 2013).

Comparison of mixotrophic and heterotrophic growth of *C. ljungdahlii* WT and OTA1 followed the same pattern as *C. autoethanogenum* WT and mutant strain described in Liew et al. 2016b (Fig. 1a). That is, both mutants had lower growth under heterotrophic conditions and about the same growth under mixotrophic conditions (Liew et al. 2016b) (Table 3). While Liew et al. discussed recapture of CO₂ being the mechanism for higher growth of WT *C. autoethanogenum*, here new insights on mixotrophic growth are discussed. Though WT cells were able to recapture more CO₂ than OTA1 cells because of a functional Wood-Ljungdahl pathway operating in WT cells, comparison of the amount of CO₂ produced by each strain under heterotrophic conditions to the amount they produced under mixotrophic conditions revealed that the addition of CO and H₂ did not improve CO₂ fixation by WT or OTA1. In other words, the amount of CO (mols) consumed by each strain was about the same as the amount of CO₂ produced (mols) (data not shown). This indicates that *C. ljungdahlii* was neither utilizing the reduced electron carriers generated from CO dehydrogenase (CO oxidizing, not acetyl-CoA synthase) or hydrogenase enzymes (reduced ferredoxin and NADPH) to fix more CO₂ nor utilizing the additional CO as a substrate for the acetyl-CoA synthase enzyme complex. Instead, based on higher biomass yields for mixotrophic fermentations compared to the heterotrophic fermentations, reduced ferredoxin and NADPH resulting from electrons donated by CO and H₂ were instead used for biomass production (Table 3). Also, the addition of CO and H₂ resulted in higher acetate yields (Fig. 1c; Table 3). Since ATP is a co-product of acetate production and used for biomass production, higher acetate yields are consistent with the higher biomass yields of mixotrophic cultures compared to

heterotrophic cultures. Furthermore, the citrate lyase beta chain, acyl lyase subunit (encoded by CLJU_c25330), and a citrate lyase acyl carrier protein, citrate lyase gamma chain (encoded by CLJU_c25340), were significantly more highly expressed in OTA1 than WT at 14 h (Table 2). Citrate lyase uses ATP to produce the anabolic building blocks oxaloacetate and acetyl-CoA from citrate for biomass production. Citrate may be formed from catabolism of amino acids or peptides from the undefined extracts and peptone used as media components in this study. While lactate and 2,3-butanediol fermentation products were not measured in this study, Liew et al. found that these products were higher for the *C. autoethanogenum* AcsA mutant grown under heterotrophic conditions but lower in mixotrophic conditions (Liew et al. 2016b). This is surprising since one would suspect that more reduced electron carriers would result in more of these reduced fermentation products. Yet, as with OTA1, the biomass yield of the *C. autoethanogenum* AcsA mutant increases with availability of CO and H₂. Therefore, not only is the surplus of reducing equivalents a critical factor in flux to reduced fermentation products, but also which reducing equivalents are available.

The OTA1 mutant may be a helpful tool in elucidating the electron-shuttling pathway in *C. ljungdahlii*, which has been under investigation since *C. ljungdahlii* was shown to be able to utilize electricity to reduce CO₂ (Nevin et al. 2011; Nevin et al. 2010). The electron uptake mechanism of *C. ljungdahlii* is currently unknown and expected to be significantly different compared to other electro-trophic bacteria because it cannot synthesize c-type cytochromes or quinones (Tremblay and Zhang 2015). Potential entry points for electrons in a *C. ljungdahlii* MES system include both carbon monoxide dehydrogenase and formate dehydrogenase since they are reversible electrocatalysts when attached to graphite electrodes (Bachmeier and Armstrong 2015). Since acetyl-CoA synthesis is blocked in OTA1, CO and/or formate should theoretically accumulate in an MES system as CO₂ and protons are converted to these products with electrical energy. For the same reason, H₂ should build up if it is part of the electrochemical pathway. Using the OTA1 strain, which has an inactive Wood-Ljungdahl pathway, for electrocatalysis, studies can save research time by avoiding the need for making knockout mutants.

Besides being a useful mutant for research, the OTA1 strain may also be valuable for some industrial applications. An example platform previously mentioned is the carboxylate platform, which has process stages including primary fermentation of waste to make short-chain fatty acids and alcohols as well as a process stage that converts medium-chain fatty acids to alcohols (Agler et al. 2012; Agler et al. 2011). The OTA1 strain may be a good fit for the second stage if its AOR can reduce medium-chain fatty acids to alcohols. Unlike WT, CO supplied to OTA1 would only be used as an electron source, not a carbon source, so more flux control is possible. Also, in this study,

OTA1 biocomposites were shown to oxidize CO faster than WT (Fig. 6). Since WT cells have two CO utilizing activities (CO oxidation and acetyl-CoA synthesis), but OTA1 only has one activity (CO oxidation), it is unclear why this is the case. It is possible that CO oxidase gene expression was higher for OTA1 compared to WT, but investigation of the physiological states of the cells on biocomposites was beyond the scope of this study. What is clear is that CO oxidation is faster for OTA1 compared to WT, and CO can only be utilized as an electron source. This combination may benefit the rate of medium-chain fatty acid reduction in the carboxylate platform.

In conclusion, this study demonstrates that the *C. ljungdahlii* OTA1 strain has an inoperable Wood-Ljungdahl pathway preventing autotrophic growth. However, mixotrophic growth of OTA1 increases the ethanol to acetate ratio and CO₂ production compared to WT, and a SNP in the *AcsA* gene explains all of these phenotypic changes. The mutations in the *ADI* and *DeoR* transcriptional regulators and *HemL* have more minor or no effect on growth and fermentation products. Investigation of the OTA1 strain has contributed new insights into *C. ljungdahlii*'s physiology and metabolism, which can be extended to closely related species, and the newly discovered properties of this strain offer new potential for further study and industrial application.

Acknowledgments The authors would like to thank Dr. Jimmy Gosse for contributing to the gas chromatography instrumentation and protocol development and Dr. Sarwat Khattak for the use of the Nova BioProfile 400 Analyzer.

Compliance with ethical standards

Funding This study is based upon work supported in whole or part by the North Carolina Biotechnology Center (NCBC) (award no. 2008-MRG-1104). Any opinion, findings, conclusions, or recommendations expressed in this publication are those of the authors and do not necessarily reflect the views and policies of the NCBC. Funding for JW was provided by a USDA National Needs Fellowship (NNF award no. 2010-38420-20399).

Conflict of interest The authors declare that they have no conflict of interest.

Ethical approval This article does not contain any studies with human participants or animals performed by any of the authors.

References

- Agler MT, Spirito CM, Usack JG, Werner JJ, Angenent LT (2012) Chain elongation with reactor microbiomes: upgrading dilute ethanol to medium-chain carboxylates. *Energy Environ Sci* 5:8189–8192
- Agler MT, Wrenn BA, Zinder SH, Angenent LT (2011) Waste to bioproduct conversion with undefined mixed cultures: the carboxylate platform. *Trends Biotechnol* 29:70–78
- Bachmeier A, Armstrong F (2015) Solar-driven proton and carbon dioxide reduction to fuels—lessons from metalloenzymes. *Curr Opin Chem Biol* 25:141–151
- Banerjee A, Leang C, Ueki T, Nevin KP, Lovley DR (2014) Lactose-inducible system for metabolic engineering of *Clostridium ljungdahlii*. *Appl Environ Microbiol* 80:2410–2416
- Barik S, Prieto S, Harrison S, Clausen E, Gaddy J (1988) Biological production of alcohols from coal through indirect liquefaction. *Appl Biochem Biotechnol* 18:363–378
- Battle-Vilanova P, Puig S, Gonzalez-Olmos R, Balaguer MD, Colprim J (2015) Continuous acetate production through microbial electrosynthesis from CO₂ with microbial mixed culture. *J Chem Technol Biotechnol* doi:10.1002/jctb.4657
- Bengelsdorf FR, Poehlein A, Linder S, Erz C, Hummel T, Hoffmeister S, Daniel R, Dürre P (2016) Industrial acetogenic biocatalysts: a comparative metabolic and genomic analysis. *Front Microbiol* 7:1036. doi:10.3389/fmicb.2016.01036 eCollection 2016
- Benjamini Y, Hochberg Y (1995) Controlling the false discovery rate: a practical and powerful approach to multiple testing. *J R Stat Soc Series B Stat Methodol* 57:289–300
- Bornstein BJ, Keating SM, Jouraku A, Hucka M (2008) LibSBML: an API library for SBML. *Bioinformatics* 24:880–881
- Bruno-Barcena J, Chinn MS, Grunden AM (2013) Genome sequence of the autotrophic acetogen *Clostridium autoethanogenum* JA1-1 strain DSM 10061, a producer of ethanol from carbon monoxide. *Genome Announc* 1:e00628–e00613
- Buckel W, Thauer RK (2013) Energy conservation via electron bifurcating ferredoxin reduction and proton/Na(+) translocating ferredoxin oxidation. *Biochim Biophys Acta* 1827:94–113. doi:10.1016/j.bbabi.2012.07.002
- Cotter JL, Chinn MS, Grunden AM (2009a) Ethanol and acetate production by *Clostridium ljungdahlii* and *Clostridium autoethanogenum* using resting cells. *Bioprocess Biosyst Eng* 32:369–380
- Cotter JL, Chinn MS, Grunden AM (2009b) Influence of process parameters on growth of *Clostridium ljungdahlii* and *Clostridium autoethanogenum* on synthesis gas. *Enzym Microb Technol* 44:281–288
- Daniell J, Köpke M, Simpson SD (2012) Commercial biomass syngas fermentation. *Energies* 5:5372–5417
- de Sanctis D, McVey CE, Enguita FJ, Carrondo MA (2009) Crystal structure of the full-length sorbitol operon regulator SorC from *Klebsiella pneumoniae*: structural evidence for a novel transcriptional regulation mechanism. *J Mol Biol* 387:759–770
- Drake HL (1994) Acetogenesis, acetogenic bacteria, and the acetyl-CoA “Wood/Ljungdahl” pathway: past and current perspectives. *Acetogenesis*. Springer, New York, pp. 3–60
- Eswar N, Webb B, Marti-Renom MA, Madhusudhan M, Eramian D, Shen MY, Pieper U, Sali A (2006) Comparative protein structure modeling using Modeller. *Curr Protoc Bioinformatics*: 5.6. 1–5.6. 30
- Fast AG, Papoutsakis ET (2012) Stoichiometric and energetic analyses of non-photosynthetic CO₂-fixation pathways to support synthetic biology strategies for production of fuels and chemicals. *Curr Opin Chem Eng* 1:380–395
- Ge H, Lv X, Fan J, Gao Y, Teng M, Niu L (2010) Crystal structure of glutamate-1-semialdehyde aminotransferase from *Bacillus subtilis* with bound pyridoxamine-5'-phosphate. *Biochem Biophys Res Commun* 402:356–360
- Gosse JL, Chinn MS, Grunden AM, Bernal OI, Jenkins JS, Yeager C, Kosourov S, Seibert M, Flickinger MC (2012) A versatile method for preparation of hydrated microbial-latex biocatalytic coatings for gas absorption and gas evolution. *J Ind Microbiol Biotechnol* 39:1269–1278
- Hoofst R, Vriend G, Sander C, Abola EE (1996) Errors in protein structures. *Nature* 381:272–272
- Ilag LL, Jahn D (1992) Activity and spectroscopic properties of the *Escherichia coli* glutamate 1-semialdehyde aminotransferase

- and the putative active site mutant K265R. *Biochemistry* 31: 7143–7151
- Jeoung JH, Dobbek H (2009) Structural basis of cyanide inhibition of Ni, Fe-containing carbon monoxide dehydrogenase. *J Am Chem Soc* 131:9922–9923
- Keating SM, Bornstein BJ, Finney A, Hucka M (2006) SBMLToolbox: an SBML toolbox for MATLAB users. *Bioinformatics* 22:1275–1277
- King ZA, Dräger A, Ebrahim A, Sonnenschein N, Lewis NE, Palsson BO (2015) Escher: a web application for building, sharing, and embedding data-rich visualizations of biological pathways. *PLoS Comput Biol* 11:e1004321
- Köpke M, Held C, Hujer S, Liesegang H, Wiezer A, Wollherr A, Ehrenreich A, Liebl W, Gottschalk G, Dürre P (2010) *Clostridium ljungdahlii* represents a microbial production platform based on syngas. *Proc Natl Acad Sci U S A* 107:13087–13092
- Köpke M, Mihalcea C, Liew FM, Tizard JH, Ali MS, Conolly JJ, Al-Sinawi B, Simpson SD (2011) 2,3-Butanediol production by acetogenic bacteria, an alternative route to chemical synthesis, using industrial waste gas. *Appl Environ Microbiol* 77:5467–5475
- Krug M, Lee SJ, Boos W, Diederichs K, Welte W (2013) The three-dimensional structure of TrmB, a transcriptional regulator of dual function in the hyperthermophilic archaeon *Pyrococcus furiosus* in complex with sucrose. *Prot Sci* 22:800–808
- Laskowski RA, Rullmann JA, MacArthur MW, Kaptein R, Thornton JM (1996) AQUA and PROCHECK-NMR: programs for checking the quality of protein structures solved by NMR. *J Biomol NMR* 8:477–486
- Leang C, Ueki T, Nevin KP, Lovley DR (2013) A genetic system for *Clostridium ljungdahlii*: a chassis for autotrophic production of biocommodities and a model homoacetogen. *Appl Environ Microbiol* 79:1102–1109
- Liew F, Martin ME, Tappel RC, Heijstra BD, Mihalcea C, Köpke M (2016a) Gas fermentation—a flexible platform for commercial scale production of low-carbon-fuels and chemicals from waste and renewable feedstocks. *Front Microbiol* 7:694. doi:10.3389/fmicb.2016.00694 eCollection 2016
- Liew F, Henstra AM, Winzer K, Köpke M, Simpson SD, Minton NP (2016b) Insights into CO₂ fixation pathway of *Clostridium autoethanogenum* by targeted mutagenesis. *MBio* 7:e00427–e00416
- Liu J, Tan Y, Yang X, Chen X, Li F (2013) Evaluation of *Clostridium ljungdahlii* DSM 13528 reference genes in gene expression studies by qRT-PCR. *J Biosci Bioeng* 116:460–464
- Lovley DR (2011) Powering microbes with electricity: direct electron transfer from electrodes to microbes. *Environ Microbiol Rep* 3:27–35
- Lovley DR, Nevin KP (2011) A shift in the current: new applications and concepts for microbe-electrode electron exchange. *Curr Opin Biotechnol* 22:441–448
- Milne I, Stephen G, Bayer M, Cock P, Pritchard L, Cardle L, Shaw PD, Marshall D (2012) Using tablet for visual exploration of second-generation sequencing data. *Briefings Bioinform* 14:193–202. doi:10.1093/bib/bbs012
- Mock J, Zheng Y, Mueller AP, Ly S, Tran L, Segovia S, Nagaraju S, Köpke M, Durre P, Thauer RK (2015) Energy conservation associated with ethanol formation from H₂ and CO₂ in *Clostridium autoethanogenum* involving electron bifurcation. *J Bacteriol* 197: 2965–2980
- Nagarajan H, Sahin M, Nogales J, Latif H, Lovley D, Ebrahim A, Zengler K (2013) Characterizing acetogenic metabolism using a genome-scale metabolic reconstruction of *Clostridium ljungdahlii*. *Microb Cell Factories* 12:118
- Nevin KP, Hensley SA, Franks AE, Summers ZM, Ou J, Woodard TL, Snoeyenbos-West OL, Lovley DR (2011) Electrosynthesis of organic compounds from carbon dioxide is catalyzed by a diversity of acetogenic microorganisms. *Appl Environ Microbiol* 77:2882–2886
- Nevin KP, Woodard TL, Franks AE, Summers ZM, Lovley DR (2010) Microbial electrosynthesis: feeding microbes electricity to convert carbon dioxide and water to multicarbon extracellular organic compounds. *MBio* 1:e00103–e00110
- Perez JM, Richter H, Loftus SE, Angenent LT (2013) Biocatalytic reduction of short-chain carboxylic acids into their corresponding alcohols with syngas fermentation. *Biotechnol Bioeng* 110:1066–1077
- Ragsdale SW, Pierce E (2008) Acetogenesis and the Wood-Ljungdahl pathway of CO₂ fixation. *BBA Proteins Proteom* 1784:1873–1898
- Richter H, Molitor B, Wei H, Chen W, Aristilde L, Angenent LT (2016) Ethanol production in syngas-fermenting *Clostridium ljungdahlii* is controlled by thermodynamics rather than by enzyme expression. *Energy Environ Sci* 9:2392–2399
- Rosenbaum MA, Henrich AW (2014) Engineering microbial electrocatalysis for chemical and fuel production. *Curr Opin Biotechnol* 29:93–98
- Schellenberger J, Que R, Fleming RM, Thiele I, Orth JD, Feist AM, Zielinski DC, Bordbar A, Lewis NE, Rahmanian S (2011) Quantitative prediction of cellular metabolism with constraint-based models: the COBRA Toolbox v2.0. *Nat Protoc* 6:1290–1307
- Schuchmann K, Müller V (2014) Autotrophy at the thermodynamic limit of life: a model for energy conservation in acetogenic bacteria. *Nature Rev Microbiol* 12:809–821
- Schulte MJ, Wiltgen J, Ritter J, Mooney CB, Flickinger MC (2016) A high gas fraction, reduced power, syngas bioprocessing method demonstrated with a *Clostridium ljungdahlii* OTA1 paper biocomposite. *Biotechnol Bioeng*. doi:10.1002/bit.25966
- Shen MY, Sali A (2006) Statistical potential for assessment and prediction of protein structures. *Prot Sci* 15:2507–2524
- Tanner RS, Miller LM, Yang D (1993) *Clostridium ljungdahlii* sp. nov., an acetogenic species in clostridial rRNA homology group I. *Int J Syst Bacteriol* 43:232–236
- Tirado-Acevedo O (2010) Ph.D. thesis. North Carolina State University, Raleigh, NC. Production of bioethanol from synthesis gas using *Clostridium ljungdahlii* as a microbial catalyst.
- Tremblay PL, Zhang T, Dar SA, Leang C, Lovley DR (2012) The Rnf complex of *Clostridium ljungdahlii* is a proton-translocating ferredoxin:NAD⁺ oxidoreductase essential for autotrophic growth. *MBio* 4:e00406–e00412
- Tremblay PL, Zhang T (2015) Electrifying microbes for the production of chemicals. *Front Microbiol* 6:201
- Vasudevan D, Richter H, Angenent LT (2014) Upgrading dilute ethanol from syngas fermentation to n-caproate with reactor microbiomes. *Bioresour Technol* 151:378–382
- Wang S, Huang H, Kahnt J, Mueller AP, Köpke M, Thauer RK (2013) NADP-specific electron-bifurcating [FeFe]-hydrogenase in a functional complex with formate dehydrogenase in *Clostridium autoethanogenum* grown on CO. *J Bacteriol* 194:4373–4386. doi:10.1128/JB.00678-13
- Whitham JM, Tirado-Acevedo O, Chinn MS, Pawlak JJ, Grunden AM (2015) Metabolic response of *Clostridium ljungdahlii* to oxygen exposure. *Appl Environ Microbiol* 81:8379–8391. doi:10.1128/AEM.02491-15
- Whitham JM, Pawlak JJ, Grunden AM (2016) *Clostridium ljungdahlii*: a review of the development of an industrial biocatalyst. *Current Biotechnology* 5:54–70
- Zelbuch L, Lindner SN, Zegman Y, Slutskiy IY, Antonovsky N, Gleizer S, Milo R, Bar-Even A (2016) Pyruvate formate-lyase enables efficient growth of *Escherichia coli* on acetate and formate. *Biochemistry* 55:2423–2426